analytical chemistry

pubs.acs.org/ac Article

Detection of Acetylcholine at Nanoscale NPOE/Water Liquid/Liquid Interface Electrodes

Henry D. Jetmore, Conrad B. Milton, Edappalil Satheesan Anupriya, Ran Chen, Kerui Xu, and Mei Shen*

Cite This: https://doi.org/10.1021/acs.analchem.1c03711 Read Online

ACCESS | Metrics & More | Article Recommendations | Supporting Information

ABSTRACT: The interface between two immiscible electrolyte solutions (ITIES) has become a very powerful analytical platform for sensing a diverse range of chemicals (e.g., metal ions and neurotransmitters) with the advantage of being able to detect non-redox electroactive species. The ITIES is formed between organic and aqueous phases. Organic solvent identity is crucial to the detection characteristics of the ITIES [half-wave transfer potential ($E_{1/2}$), potential window range, limit of detection, transfer coefficient (α), standard heterogeneous ion-transfer rate constant (k^0), etc.]. Here, we demonstrated, for the first time at the nanoscale, the detection characteristics of the NPOE/water ITIES. Linear detection of the diffusion-limited current at different concentrations of acetylcholine (ACh) was demonstrated with cyclic voltammetry (CV) and $i-t$ amperometry. The $E_{1/2}$ of ACh transfer at the NPOE/water nanoITIES was -0.342 ± 0.009 V versus the $E_{1/2}$ of tetrabutylammonium (TBA^+). The limit of detection of ACh at the NPOE/water nanoITIES was 37.1 ± 1.5 μM for an electrode with a radius of ~127 nm. We also determined the ion-transfer kinetics parameters, α and k^0, of TBA^+ at the NPOE/water nanoITIES by fitting theoretical cyclic voltammograms to experimental voltammograms. This work lays the basis for future cellular studies using ACh detection at the nanoscale and for studies to detect other analytes. The NPOE/water ITIES offers a potential window distinct from that of the 1,2-dichloroethane (DCE)/water ITIES. This unique potential window would offer the ability to detect analytes that are not easily detected at the DCE/water ITIES.

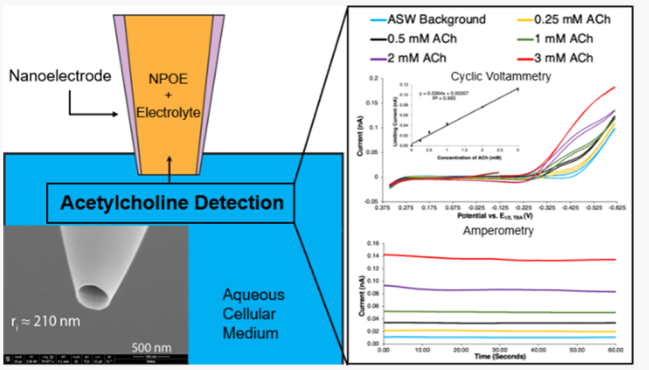

INTRODUCTION

The interface between two immiscible electrolyte solutions (ITIES) has become a powerful analytical platform for sensing a wide range of chemicals (e.g., metal ions, neurotransmitters, and proteins), with an advantage being the ability to detect non-redox electroactive analytes.[1−26] An ITIES experimental setup is commonly composed of two phases of low mutual miscibility, where one phase is aqueous and the other phase is a polar organic solvent with a moderate or high dielectric permittivity.[27] Marcus proposed an ion-transfer theory for the ITIES based on the recognition that an ion undergoes initial desolvation from the first phase that is accompanied by concerted solvation into the second phase.[28] The organic solvent, as a part of the ITIES structure, plays a critical role in electrochemical reactions at the ITIES.[26,29] Therefore, optimal conditions for detecting different species can be obtained by varying the organic solvent. Additionally, developing new systems at the nanoscale will enable new fundamental studies and applications.

In recent years, the development of nanoscale ITIES (nanoITIES) platforms has enabled chemical analysis with a high spatial resolution. While different organic solvents have been reported in nanoITIES studies, including ionic liquids,[30] octanol,[23] DCE,[3,6,31,32] and true oils (i.e., avocado oil, coconut oil, and walnut oil),[29] NPOE has not been explored as the organic solvent for nanoITIES studies. NPOE has been used for the detection of ionic species at the macro- and microscales.[33−48] Here, we demonstrate the detection of an analyte at the NPOE/water nanoITIES using the neurotransmitter acetylcholine (ACh) as one example.

ACh is of widespread interest because of its role in neuronal function and disorders. ACh is involved in the chemical transmission at synapses and performs functions such as regulating other neurotransmitters, controlling the opening of ligand-gated ion channels, and facilitating bursts of neuronal

Received: August 27, 2021
Accepted: October 28, 2021

firing.[49] Imbalances of ACh levels have been linked to Alzheimer's disease, myasthenia gravis, as well as behavioral, learning, and sleep disorders.[50−53] Enzymatic detection of ACh has been achieved by the sequential use of acetylcholinesterase and choline oxidase to generate hydrogen peroxide from ACh.[54−77] ACh quantification is then achieved by electrochemical or optical detection of the hydrogen peroxide,[77,78] but other methods have also been used.[79−82] ACh has also been detected using a nickel anode electrode[83] and electrodes that were modified with only acetylcholinesterase.[84−91] So far, all of these have been carried out at micro- and macroscales.

Here, we report the first-ever analyte detection at NPOE/water nanoITIES electrodes. We also performed a study of the kinetics of the transfer of tetrabutylammonium (TBA^+) across the NPOE/water interface. Despite NPOE having high viscosity, sigmoidal cyclic voltammograms from the detection of ACh were observed.[92] The NPOE/water nanoITIES offers a unique potential window compared to other nanoITIES systems. The rate constant of TBA^+ transfer is sufficiently fast despite the high viscosity of NPOE. Cyclic voltammetry (CV) and $i-t$ amperometry showed linear responses of the diffusion-limited current as the concentration of ACh was varied.

EXPERIMENTAL SECTION

Reagents. Sodium chloride (NaCl) was from EMD Chemicals (Gibbstown, NJ). Potassium chloride (KCl) was from VWR International (Radnor, PA). Magnesium chloride hexahydrate ($MgCl_2·6H_2O$) was from Amresco (Solon, OH). Magnesium sulfate ($MgSO_4$) and 4-(2-hydroxyethyl)-1-piperazineethanesulfonic acid (HEPES) were from Fisher Scientific (Pittsburgh, PA). Calcium chloride dihydrate ($CaCl_2·2H_2O$), tetradodecylammonium chloride (TDDACl), tetrabutylammonium chloride (TBACl), 1,2-dichloroethane (DCE), *N*,*N*-dimethyltrimethylsilylamine, *o*-nitrophenyl octyl ether (NPOE), tetrabutylammonium hexafluorophosphate ($TBAPF_6$), and acetylcholine chloride (AChCl, retroactively estimated hydration level 7 wt. %) were obtained from Sigma-Aldrich (St. Louis, MO). Potassium tetrakis-(pentafluorophenyl) borate (TFAB) was from Boulder Scientific Company (Mead, CO). All aqueous solutions were prepared from 18.3 MΩ cm deionized water. The artificial seawater (ASW) used was aqueous solution containing 460 mM NaCl, 10 mM KCl, 10 mM $CaCl_2$, 22 mM $MgCl_2$, 26 mM $MgSO_4$, and 10 mM HEPES (pH 7.8). The TFAB salt of TDDA (TDDATFAB) was prepared by metathesis as described elsewhere.[93]

NanoITIES Electrode Fabrication, Characterization, and Electrochemical Measurements. NanoITIES electrodes were fabricated using previously reported methods.[3,4,6,31,94] Pipettes with orifices of ∼100−300 nm radii were prepared by laser pulling quartz capillaries (Sutter Instruments Co. Novato CA; 1 mm outer diameter, 0.7 mm inner diameter, 7.5 cm length) into nanopipettes using a P-2000 Laser Puller (Sutter Instruments, Novato, CA). The inner glass surface of these nanopipettes was modified by a silanization reaction with *N*,*N*-dimethyltrimethylsilylamine vapor to convert it from hydrophilic to hydrophobic, ensuring that a flat, stable oil-water interface was formed at each nanopipette orifice during experiments. Due to the nature of the chemical vapor silanization, the outer glass surface has likely been silanized as well. For measuring the half-wave transfer potential ($E_{1/2}$), the nanopipette was backfilled with an oil solution of 0.1 M TDDATFAB dissolved in NPOE using a 10 μL Hamilton syringe. For kinetics measurements, a different filling solution was used as detailed in the section "Determination of Ion Transfer Kinetics Parameters." The solution was forced to the tip of the nanopipette using gentle vibrations. An etched Pt wire was inserted into the filled pipette as reported in previous works.[3,4,6,16,29] The tip of the nanoITIES electrode was inserted into ASW for chemical analysis. ASW was used as the aqueous phase because it is the biological cellular medium for a common neuronal model in our lab, *Aplysia californica*. By studying ion transfer in this medium, future biological work can be facilitated. Nanoelectrode radii were calculated using the TBA^+ transfer current from ASW (aqueous phase) into a pipette (oil phase) and were confirmed using the ACh transfer current from ASW into the pipette and the slope of ACh calibration curves. A scanning electron microscope (FEI Helios 600i Dual Beam SEM/FIB, FEI Co., Hillsboro, OR) was also used to visually confirm the radii of the silanized nanopipette orifices. Pipettes were coated with Au−Pd using a sputter coater (Emitech K575, Emitech Ltd., Ashford, Kent) using a 20 mA current for 40 s before SEM. Sputter coating increases the resolution of the images that can be obtained from SEM by limiting charging on the glass pipette surface to reduce the blurring of the electron image.[5] Pipettes were examined via SEM under a 2 kV electron beam.

All electrochemical measurements were performed using a CHI 760E potentiostat (CH Instruments, Austin, TX). CV was used to measure the potential window and study the ion transfer at the NPOE/water nanointerface. A two-electrode configuration was used,[3,4,6,16,29] where a potential was applied between the Pt wire inside the nanopipette and the Ag/AgCl quasi-reference electrode outside of the nanopipette. Negative potential is for the positive ion transfer from water to oil, seen as positive current, as commonly reported.[3,4,6,10,16,29,30] We standardized the $E_{1/2}$ values for ACh detection with respect to an internal standard, TBA^+, by subtracting the half-wave transfer potential of TBA^+ ($E_{1/2,\ TBA}$) from the $E_{1/2}$ of ACh.

Determination of the Positive Direction Onset Potential and the Negative Direction Onset Potential for Potential Window Analysis. The potential window for NPOE was defined as the region in which mainly the capacitive current was measured. The potential window was calculated from cyclic voltammograms of the ASW solution, which was the background for our experiments.[29] The variables used to calculate the potential window (E_{pos}, E_{neg}, i_{pos}, i_{neg}, i_{base}, and i_c) are all presented in Scheme 1. We define the potential window as the difference between the onset potential of the voltammogram in the positive direction (E_{pos}) and the onset potential of the voltammogram in the negative direction (E_{neg}). E_{pos} is defined as the potential in the lower capacitive trace that corresponds to i_{pos}, where $i_{pos} = i_{base} - 5|i_c|$. Similarly, E_{neg} is defined as the potential in the upper capacitive trace that corresponds to i_{neg}, where $i_{neg} = i_{base} + 5|i_c|$. i_{base}, the baseline current, is defined as the average of the current of the upper and lower current traces in the capacitive current region. The capacitive current, i_c, is defined as half of the absolute difference of the current gap between the upper and lower current traces in the capacitive current region. The calculated values of E_{pos} and E_{neg} were standardized against $E_{1/2,\ TBA}$ to give $E_{pos\ vs\ TBA}$ and $E_{neg\ vs\ TBA}$, respectively. The potential window was calculated as the difference $E_{pos\ vs\ TBA} - E_{neg\ vs\ TBA}$.

Determination of Half-Wave Transfer Potentials. $E_{1/2}$ values were determined for the analyte (ACh) through

https://doi.org/10.1021/acs.analchem.1c03711
Anal. Chem. XXXX, XXX, XXX−XXX

Scheme 1. Determination of the Onset Potential of the Voltammogram in the Positive Direction (E_{pos}) and the Onset Potential of the Voltammogram in the Negative Direction (E_{neg}) to Identify the Potential Window of the NPOE/Water NanoITIES[a]

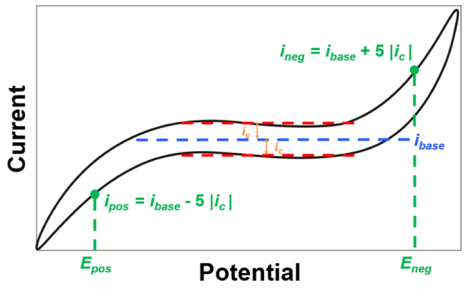

[a]Definitions are shown for the baseline current (i_{base}), the capacitive current (i_c), the positive (i_{pos}) and negative (i_{neg}) onset currents, and the positive (E_{pos}) and negative (E_{neg}) onset potentials.

concentration-dependent CV experiments. First, nanoITIES electrodes were prepared as in the section "NanoITIES Electrode Fabrication, Characterization, and Electrochemical Measurements" and inserted into the ASW solution. Three replicate cyclic voltammograms were then obtained within the potential window for different concentrations of ACh (0 [background], 0.25, 0.5, 1, 2, and 3 mM ACh in ASW). The increments of ACh were achieved by a series of additions of 0.4 M AChCl to the ASW solution. Each set of three replicates was averaged. The average background voltammogram was subtracted from each of the average voltammograms showing the detection of ACh.

The diffusion-limited region of ACh detection at the NPOE/water nanoITIES had a slight overlap with the ASW background current, so a well-defined steady-state current was not observed for ACh detection. The background-subtracted voltammograms had a peak shape and the diffusion-limited currents for each concentration of ACh were taken as the peak current of the forward wave of each background-subtracted voltammogram. Amperomograms were collected at the potential corresponding to the diffusion-limited current. At least three replicate amperomograms were collected and averaged for each concentration of ACh. The averaging was performed over the last 30 s of the amperomograms.

After voltammograms were obtained for all the ACh concentrations, to standardize the results, 0.4 M TBACl was added to the ASW solution to increase the concentration of TBA^+ to 1 mM. Again, three replicate voltammograms were obtained, averaged, and had the ASW background subtracted from them. We subtracted $E_{1/2,\,TBA}$ from the $E_{1/2}$ for ACh to report the $E_{1/2}$ of ACh with respect to that of TBA^+.

Determination of Ion-Transfer Kinetics Parameters. The transfer coefficient (α) and the standard heterogeneous ion-transfer rate constant (k^0) were determined by fitting theoretical voltammograms produced using eq 1 to experimental voltammograms as reported previously.[29,95] First, a system was established according to Cell 1, with an electrode prepared as described in the "NanoITIES Electrode Fabrication, Characterization, and Electrochemical Measurements" section except that it was filled with an NPOE solution containing 0.1 M TDDATFAB and 5 mM $TBAPF_6$. That electrode was then inserted into a solution of ASW containing 2 mM TBACl.

Cell 1

Pt|0.1 M TDDATFAB + 5 mM TBAPF6 + NPOE ‖ASW + 2 mM TBAClIAgClIAg

$$\frac{i}{i_{ing}} = \frac{1}{\frac{m_{ing}}{m_{eg}} + \frac{m_{ing}}{k_b} + \frac{k_f}{k_b}}\left(\frac{k_f}{k_b} - \frac{c_{NPOE}}{c_w}\right) \quad (1)$$

In eq 1, i is the measured current, i_{ing} is the diffusion-limited current of ingress into the nanopipette, m_{ing} is the mass transfer coefficient of ingress, m_{eg} is the mass transfer coefficient of egress, k_f is the heterogeneous ion-transfer rate constant of ingress, k_b is the heterogeneous ion-transfer rate constant of egress, c_w is the concentration of TBA^+ in the water (w) phase, and c_{NPOE} is the concentration of TBA^+ in the oil phase. For a nanopipette, i_{ing} can be expressed as

$$i_{ing} = 4xzFD_w c_w r_i \quad (2)$$

where z is the charge on TBA^+, F is the Faraday constant, D_w is the diffusion coefficient of TBA^+ in w,[96] r_i is the inner radius of the nanopipette, and x is a parameter that is a function of the RG of the nanopipette (RG = $\frac{r_g}{r_i}$ where r_g is the outer radius of the nanopipette).[97] For the pipette used, RG = 1.4 (estimated by dividing the capillary outer radius over inner radius) and x = 1.23. Similarly, i_{eg} is described as

$$i_{eg} = 4f(\theta)zFD_{NPOE}c_{NPOE}r_i \quad (3)$$

In eq 3, D_{NPOE} is the diffusion coefficient of TBA^+ in NPOE and $f(\theta)$ is a function of the tip taper angle, θ.[98] The mass transfer coefficients m_{ing} and m_{eg} are expressed as

$$m_{ing} = \frac{4xD_w}{\pi r_i} \quad (4)$$

$$m_{eg} = \frac{4f(\theta)D_{NPOE}}{\pi r_i} \quad (5)$$

As an alternative to calculating the diffusion coefficient of TBA^+ in NPOE and $f(\theta)$, eq 3 can be rearranged and $f(\theta)\times D_{NPOE}$ can be substituted into eq 5 to yield

$$m_{eg} = \frac{i_{eg}}{zFc_{NPOE}\pi r_i^2} \quad (6)$$

Lastly, the heterogeneous ion-transfer rate constants k_f and k_b are given by the Butler–Volmer model as[27]

$$k_f = k^0 \exp\left[-\frac{\alpha zF}{RT}(\Delta\varphi - \Delta\varphi_i^{0'})\right] \quad (7)$$

$$k_b = k^0 \exp\left[\frac{(1-\alpha)zF}{RT}(\Delta\varphi - \Delta\varphi_i^{0'})\right] \quad (8)$$

where $\Delta\varphi$ is the Galvani potential difference between NPOE and water, R is the ideal gas constant, and $\Delta\varphi_i^{0'}$ is the formal transfer potential of TBA^+. The formal transfer potential of TBA^+ can be determined from the potential at which zero current is measured, or the potential at which the transfer of TBA^+ across the NPOE/water nanointerface is at equilibrium, $\Delta\varphi_{eq}$. Using $\Delta\varphi_{eq}$, $\Delta\varphi_i^{0'}$ can be described as

$$\Delta\varphi_i^{0'} = \Delta\varphi_{eq} - \frac{RT}{zF}\ln\frac{c_w}{c_{NPOE}} \quad (9)$$

https://doi.org/10.1021/acs.analchem.1c03711
Anal. Chem. XXXX, XXX, XXX−XXX

The defined parameters used in the simulation are presented in Table S1. With TBA^+ in both phases of the nanoITIES as in Cell 1, both i_{ing} and i_{eg} can be measured from the cyclic voltammogram. i_{ing} was measured as the current in the flat region (diffusion limited) in the negative potential region of the voltammogram. i_{eg} was measured as the current in the flat region (diffusion limited) in the positive potential region of the voltammogram. The experimentally obtained voltammograms are discussed further in the section "Kinetics Study of Ion Transfer at the NPOE/Water NanoITIES." To increase the accuracy of measuring i_{ing} and i_{eg}, the current deviation from zero inherent to the potentiostat was evaluated by measuring the current across a 100,000 MΩ resistor at 0 V and subtracting that current from the collected current data. The theoretical voltammogram was simulated using eq 1 where all the parameters were determined based on eqs 2−9. α and k^0 were determined with a detailed procedure in the Supporting Information. The values that provided good fits were used to determine the averages and standard deviations of α and k^0.

Limit of Detection Determination. The limit of detection (LOD) of ACh in ASW was calculated based on the method described in the Quantitative Chemical Analysis textbook, using the equation:[99]

$$\mathrm{LOD} = \frac{3s}{o} \tag{10}$$

In eq 10, s equals the standard deviation of the current measured from three replicate scans of the background ASW solution at the potential corresponding to the diffusion-limited current and o is the slope of the plot of the concentration of ACh versus the diffusion-limited current.[4]

RESULTS AND DISCUSSION

Evaluation of the Potential Window at the NPOE/Water NanoITIES. To the best of our knowledge, the potential window at the NPOE/water nanointerface (Cell 2) has not been quantitatively reported before. The potential window and the associated values of E_{pos} and E_{neg} are crucial parameters to know because they provide information about whether an analyte is likely to be detected by a given electrode. We quantified this potential window using the process described in the section "Determination of the Positive Direction Onset Potential and the Negative Direction Onset Potential for Potential Window Analysis" and illustrated in Scheme 1 using the cyclic voltammograms in Figure 1A. E_{pos} and E_{neg} were standardized against the experimentally measured half wave transfer potential of TBA ($E_{1/2,\ TBA}$) to give $E_{pos\ vs\ TBA}$ = 0.260 ± 0.036 V and $E_{neg\ vs\ TBA}$ = −0.400 ± 0.020 V, respectively. The difference in $E_{pos\ vs\ TBA}$ and $E_{neg\ vs\ TBA}$ was reported as a potential window of 0.660 ± 0.035 V. The values of $E_{pos\ vs\ TBA}$, $E_{neg\ vs\ TBA}$, and the potential window are summarized in Table 1. These reported values were obtained by averaging the calculated values of $E_{pos\ vs\ TBA}$, $E_{neg\ vs\ TBA}$, and the potential window from ASW background cyclic voltammograms obtained using four different electrodes.

Direct comparison of $E_{pos\ vs\ TBA}$, $E_{neg\ vs\ TBA}$, and the potential window of the NPOE/water nanoITIES with other studies at the NPOE/water liquid/liquid interface is difficult because results in the literature have only reported NPOE/water liquid/liquid interfaces on the macro- or microscale. In addition, these studies used different supporting electrolytes in their oil phases than the 0.1 M TDDATFAB we used and had different ions in their aqueous phases than those present in ASW.[33,34,36−39,43−46,100,101] Thus, we compared the potential window of the NPOE/water nanoITIES (Cell 2) to that of the DCE/water nanoITIES (Cell 3), considering that the DCE/water nanoITIES has been established as a powerful platform for detecting cholinergic transmitters from living neurons.[31] The results are presented in Figure 1A (NPOE/water) and 1B (DCE/water). The same quantification as with the NPOE/water interface was performed for the DCE/water interface, yielding $E_{pos\ vs\ TBA}$ = 0.023 ± 0.049 V, $E_{neg\ vs\ TBA}$ = −0.534 ± 0.068 V, and a potential window of 0.556 ± 0.055 V. The NPOE/water nanoITIES appears to have a slightly larger potential window (0.660 ± 0.035 V) compared to that of the DCE/water nanoITIES (0.556 ± 0.055 V). In addition, the $E_{pos\ vs\ TBA}$ and $E_{neg\ vs\ TBA}$ at the NPOE/water nanoITIES were more positive than the $E_{pos\ vs\ TBA}$ and $E_{neg\ vs\ TBA}$ at the DCE/water nanoITIES. This difference suggests that the NPOE/water nanoITIES will be more advantageous than DCE for detecting ions that transfer at more positive potentials.

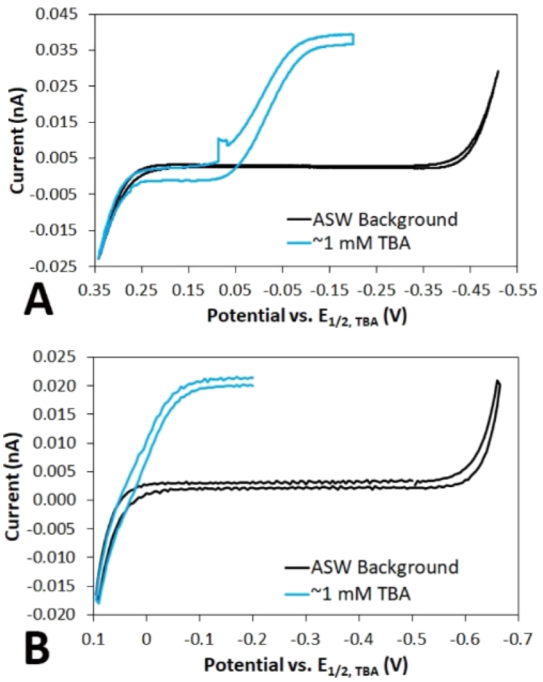

Figure 1. Potential window determination at the NPOE/water nanoITIES and the DCE/water nanoITIES. Cyclic voltammograms of the ASW background before (black) and after (blue) the addition of ~1 mM TBA^+ at the (A) NPOE/water nanoITIES and (B) DCE/water nanoITIES.

Table 1. $E_{pos\ vs\ TBA}$, $E_{neg\ vs\ TBA}$, and the Potential Window for the NPOE/Water NanoITIES (Cell 2)

$E_{pos\ vs\ TBA}$/V	Eneg vs TBA/V	potential window/V
0.260 ± 0.036 (N = 4)	−0.400 ± 0.020 (N = 4)	0.660 ± 0.035 (N = 4)

Cell 2

Pt|0.1 M TDDATFAB (electrolyte) + NPOE||ASW|AgCl|Ag

Cell 3

Pt|5 mM TDDATFAB (electrolyte) + DCE||ASW|AgCl|Ag

Detection of Acetylcholine at the NPOE/Water NanoITIES. Once the well-defined potential window was

https://doi.org/10.1021/acs.analchem.1c03711
Anal. Chem. XXXX, XXX, XXX−XXX

observed, we demonstrated, for the first time at the nanoscale, the detection of an analyte at the NPOE/water ITIES, using ACh as an example. We used the setup shown in Figure 2, and

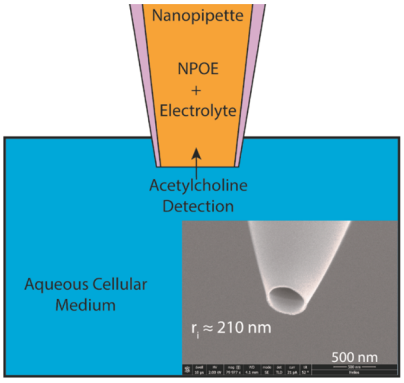

Figure 2. Experimental configuration for detection of acetylcholine at the NPOE/water nanoITIES. Inset: SEM image of a nanopipette with the approximate radius.

the procedures described in the section "Determination of Half-Wave Transfer Potentials" for this detection. Concentration-dependent detection of ACh was achieved at the NPOE/water nanoITIES using both CV and $i-t$ amperometry. The cyclic voltammograms (Figure 3A) were observed to be sigmoidal, as expected for nanoelectrodes.[92] We determined

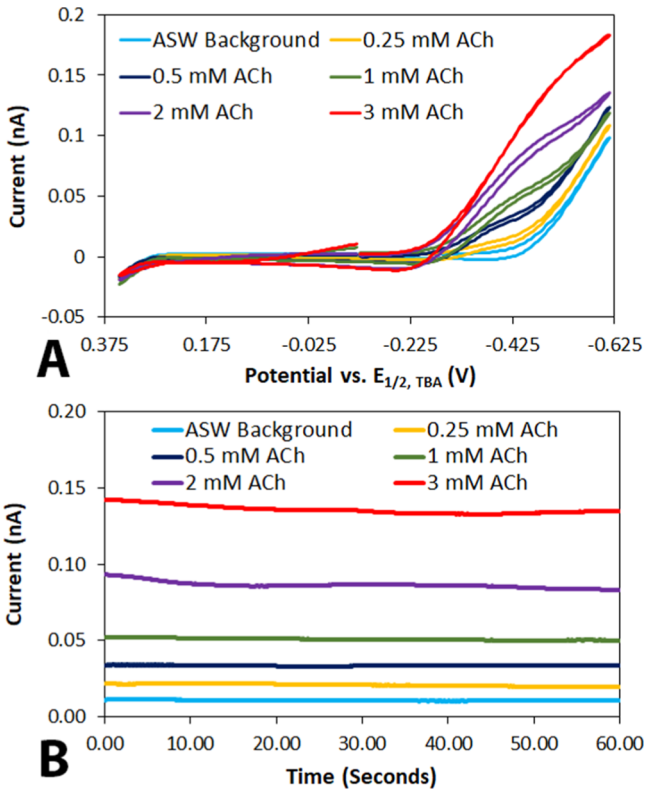

Figure 3. *In vitro* concentration-dependent acetylcholine (ACh) detection using CV (A) and $i-t$ amperometry (B) at the NPOE/water nanoITIES. The concentrations of ACh were increased from 0 to 3 mM. $i-t$ data were collected at diffusion-limited potentials of −0.33 V (ASW background), −0.32 V (0.25 mM ACh), −0.32 V (0.5 mM ACh), −0.32 V (1 mM ACh), −0.34 V (2 mM ACh), and −0.38 V (3 mM ACh).

ACh to have an $E_{1/2}$ of −0.342 ± 0.009 V versus $E_{1/2,\ TBA}$ at the NPOE/water interface. Previously, ACh was determined to have an $E_{1/2}$ of −0.11 V for its transfer from ASW solution to DCE relative to the $E_{1/2}$ of tetraethylammonium.[94]

These voltammograms also showed an expected linear trend of increasing current with increasing concentration of ACh. We obtained the diffusion-limited currents from the voltammograms as described in the section "Determination of Half-Wave Transfer Potentials" and plotted them versus the concentration of ACh in ASW (Figure S1A) to confirm that the increase in current with increasing concentration of ACh was linear. The resulting plot showed a strong linear relationship based on the R^2 value of 0.993, confirming the linear detection of ACh at the NPOE/water nanoITIES. The LOD for ACh detection was calculated to be 37.1 ± 1.5 μM at an electrode with a radius of ∼127 nm. Electrode radius was determined by averaging three separate radii calculations using three different methods (1) the TBA^+ diffusion-limited current, (2) the slope of the calibration curve constructed based on the diffusion-limited current of ACh, and (3) the average of all the radii calculated from the diffusion-limited current of each individual ACh concentration.[3−5,29]

Because CV yielded a linear relationship between the current and concentration of ACh, a similar linear relationship would be expected to be obtained with $i-t$ amperometry. Amperometry data were collected as described in the section "Determination of Half-Wave Transfer Potentials", and the amperomograms (Figure 3B), like the cyclic voltammograms, showed the expected linear trend of increasing current with increasing concentrations of ACh. To confirm the linearity of the amperometric relationship between the current and concentration of ACh, the average currents from the last 30 s of the amperomograms were plotted versus the ACh concentration in ASW (Figure S1B). The resulting plot, as with the plot obtained using CV data, showed a strong linear relationship based on an R^2 value of 0.996. Another important observation from these amperomograms was that the current at each concentration of ACh reached a stable state, showing that amperometry data obtained at the NPOE/water nanoITIES could be used to quantify the concentration of ACh, which is a crucial characteristic to applying the NPOE-based nanoITIES platform to cellular studies.

Kinetics Study of Ion Transfer at the NPOE/Water NanoITIES. We used CV to determine the kinetics of ion transfer, specifically of TBA^+, at the NPOE/water nanoITIES, based on well-established methods by the Mirkin and Amemiya groups.[95,98,102] The detailed procedures were described in the section "Determination of Ion Transfer Kinetics Parameters." Briefly, using eqs 1−9, theoretical voltammograms were generated to fit the experimental data by varying α and k^0. Figure 4 contains three overlaid experimental and theoretical voltammograms for the ingress and egress of TBA^+ transfer across the NPOE/water nanoITIES. The experimental forward wave was plotted as the solid red curve, and the theoretical forward wave curve fitting was plotted as the dashed black curve. The determined mean and standard deviation of α and k^0 are included in each plot. For an electrode with a radius of ∼215 nm (as determined from CV), α was calculated to be 0.49 ± 0.02 and k^0 was calculated to be 0.014 ± 0.002 cm/s.

Here, we compare the kinetics of TBA^+ transfer between NPOE/water nanoITIES and DCE/water nanoITIES electrodes. According to the slow interfacial diffusion model ($k^0 = D_i$/

https://doi.org/10.1021/acs.analchem.1c03711
Anal. Chem. XXXX, XXX, XXX−XXX

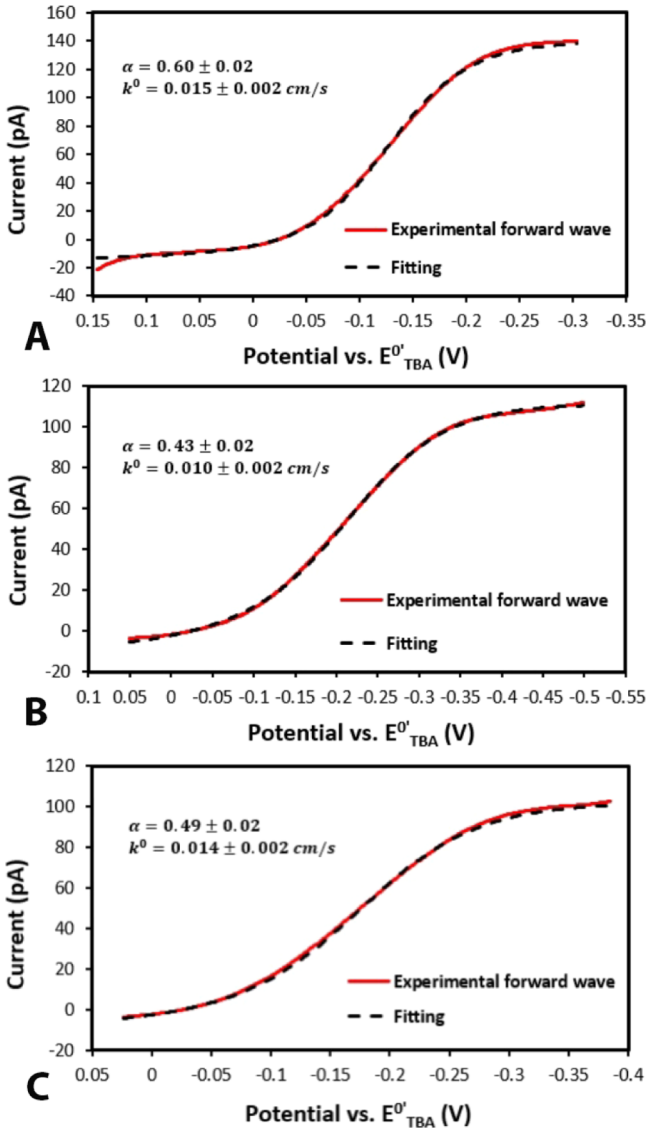

Figure 4. Determination of kinetics, transfer coefficient (α) and the standard heterogeneous ion-transfer rate constant (k^0), of TBA^+ at the NPOE/water nanoITIES. Experimental (dashed black) and fitted (red) CVs were obtained as described in the section "Determination of Ion Transfer Kinetics Parameters" for electrodes with radii of (A) ~295, (B), ~230, and (C) ~215 nm. Potential values are plotted versus the formal potential of TBA^+, $E^{0'}_{TBA}$.

Δx, where D_i is the ion's diffusion coefficient in the boundary layer and Δx is the thickness of the boundary layer),[103,104] the k^0 at the NPOE/water nanoITIES is expected to be smaller than that at the DCE/water nanoITIES based on the proposed decrease in k^0 with increasing solvent viscosity (smaller D_i).[2,29,30] Matching this theoretical prediction, the experimentally determined k^0 value for TBA^+ transfer at the NPOE/water nanoITIES was smaller than the k^0 at the DCE/water nanoITIES,[16,29] but the k^0 value at the NPOE/water nanoITIES was lower than predicted by the interfacial diffusion model. However, other factors likely play a role in explaining the smaller than expected k^0 at the NPOE/water nanoITIES. The radii of the nanoelectrodes in this study are larger than those of the nanoelectrodes in the study using DCE by a factor of ~3.5−14.4;[29] thus, the difference in kinetics parameters cannot be solely attributed to solvent viscosity. As shown by the equation $m_0 = D_i/r_i$, where m_0 is the mass-transport coefficient and r_i is the effective radius of the nanoelectrode,[105,106] the use of larger nanoelectrodes in this study would decrease the mass-transport rate of TBA^+ relative to the study of the kinetics of TBA^+ transfer at the DCE/water nanoITIES supported by smaller nanopipettes. The kinetics may also be altered by differences in the solvation energy of TBA^+ for the transfer from water to NPOE compared to DCE.[26,28,107] This difference would be an extension of the ion-transfer theory proposed by Marcus suggesting that ion-transfer reactions involve an initial desolvation from the first liquid phase followed by concerted solvation into the second liquid phase.[28] Because the solubility of NPOE in water is much smaller than the solubility of DCE in water,[37,108−110] the solvation energy would be different for the transfer of TBA^+ from water to NPOE versus the transfer of TBA^+ from water to DCE.

CONCLUSIONS

We have developed NPOE/water nanoITIES electrodes for the quantitative and qualitative detection of ACh, to the best of our knowledge, for the first time. Sigmoidal cyclic voltammograms were observed at the NPOE/water nanoITIES, and the potential window was found to be slightly larger than that of the DCE/water nanoITIES, by ~0.104 ± 0.065 V. In addition, the potential window at the NPOE/water nanoITIES is shifted to a more positive potential by ~0.186 ± 0.073 V versus the potential window at the DCE/water nanoITIES, so the NPOE/water nanoITIES can potentially detect analytes that are difficult to detect at the DCE/water nanoITIES. Linear detection of ACh was observed using both CV and $i-t$ amperometry. A kinetics study showed that ion transfer at the NPOE/water nanoITIES is rather fast despite the high viscosity of NPOE. Overall, this study lays the foundation for future cellular studies and other applications of analytical sensing with NPOE/water nanoITIES.

ASSOCIATED CONTENT

Supporting Information

The Supporting Information is available free of charge at https://pubs.acs.org/doi/10.1021/acs.analchem.1c03711.

Background regarding ITIES thermodynamics; process of determining α and k^0; kinetics simulation parameters; DCE potential window information; linear calibration curves for CV and $i-t$ amperometry ACh detection with background subtracted voltammograms; and references (PDF)

AUTHOR INFORMATION

Corresponding Author

Mei Shen − *The Beckman Institute for Advanced Science and Technology and Department of Chemistry, University of Illinois at Urbana-Champaign, Urbana, Illinois 61801, United States;* orcid.org/0000-0002-6033-8308; Email: mshen233@illinois.edu

Authors

Henry D. Jetmore − *Department of Chemistry, University of Illinois at Urbana-Champaign, Urbana, Illinois 61801, United States;* orcid.org/0000-0002-1308-1503

https://doi.org/10.1021/acs.analchem.1c03711
Anal. Chem. XXXX, XXX, XXX−XXX

Conrad B. Milton − *Department of Chemistry, University of Illinois at Urbana-Champaign, Urbana, Illinois 61801, United States;* orcid.org/0000-0002-9305-1290
Edappalil Satheesan Anupriya − *Department of Chemistry, University of Illinois at Urbana-Champaign, Urbana, Illinois 61801, United States;* orcid.org/0000-0002-5177-8280
Ran Chen − *Department of Chemistry, University of Illinois at Urbana-Champaign, Urbana, Illinois 61801, United States;* orcid.org/0000-0002-6808-4381
Kerui Xu − *Department of Chemistry, University of Illinois at Urbana-Champaign, Urbana, Illinois 61801, United States;* orcid.org/0000-0001-9666-0713

Complete contact information is available at: https://pubs.acs.org/10.1021/acs.analchem.1c03711

Author Contributions

H.D.J. and C.B.M. contributed equally. All authors have given approval to the final version of the manuscript.

Notes

The authors declare no competing financial interest.

■ ACKNOWLEDGMENTS

The SEM measurements were carried out in part in the Materials Research Laboratory Central Research Facilities, University of Illinois at Urbana-Champaign. The authors are grateful to the support to this research by a National Science Foundation CAREER Award (CHE 19-45274) to M.S. C.B.M. appreciates the support from the Summer 2021 Fred C. and Josephine C. Falkner Scholarship for Undergraduate Research through the Department of Chemistry at the University of Illinois at Urbana-Champaign.

■ REFERENCES

(1) Zhan, D.; Mao, S.; Zhao, Q.; Chen, Z.; Hu; Jing, P.; Zhang, M.; Zhu, Z.; Shao, Y. *Anal. Chem.* **2004**, *76*, 4128−4136.
(2) Shao, Y.; Girault, H. H. *J. Electroanal. Chem. Interfacial Electrochem.* **1990**, *282*, 59−72.
(3) Colombo, M. L.; McNeil, S.; Iwai, N.; Chang, A.; Shen, M. *J. Electrochem. Soc.* **2015**, *163*, H3072−H3076.
(4) Colombo, M. L.; Sweedler, J. V.; Shen, M. *Anal. Chem.* **2015**, *87*, 5095−5100.
(5) Shen, M.; Colombo, M. L. *Anal. Methods* **2015**, *7*, 7095−7105.
(6) Iwai, N. T.; Kramaric, M.; Crabbe, D.; Wei, Y.; Chen, R.; Shen, M. *Anal. Chem.* **2018**, *90*, 3067−3072.
(7) Beni, V.; Ghita, M.; Arrigan, D. W. M. *Biosens. Bioelectron.* **2005**, *20*, 2097−2103.
(8) Sairi, M.; Arrigan, D. W. M. *Talanta* **2015**, *132*, 205−214.
(9) Shao, Y.; Osborne, M. D.; Girault, H. H. *J. Electroanal. Chem. Interfacial Electrochem.* **1991**, *318*, 101−109.
(10) Shao, Y.; Mirkin, M. V. *Anal. Chem.* **1998**, *70*, 3155−3161.
(11) Evans, N. J.; Gonsalves, M.; Gray, N. J.; Barker, A. L.; Macpherson, J. V.; Unwin, P. R. *Electrochem. Commun.* **2000**, *2*, 201−206.
(12) Zhan, D.; Li, X.; Zhan, W.; Fan, F.-R. F.; Bard, A. J. *Anal. Chem.* **2007**, *79*, 5225−5231.
(13) Stockmann, T. J.; Montgomery, A.-M.; Ding, Z. *J. Electroanal. Chem.* **2012**, *684*, 6−12.
(14) Amemiya, S.; Kim, J.; Izadyar, A.; Kabagambe, B.; Shen, M.; Ishimatsu, R. *Electrochim. Acta* **2013**, *110*, 836−845.
(15) Nestor, U.; Wen, H.; Girma, G.; Mei, Z.; Fei, W.; Yang, Y.; Zhang, C.; Zhan, D. *Chem. Commun.* **2014**, *50*, 1015−1017.
(16) Puri, S. R.; Kim, J. *Anal. Chem.* **2019**, *91*, 1873−1879.
(17) Mareček, V.; Samec, Z. *Curr. Opin. Electrochem.* **2017**, *1*, 133−139.
(18) Arrigan, D. W. M.; Hackett, M. J.; Mancera, R. L. *Curr. Opin. Electrochem.* **2018**, *12*, 27−32.
(19) Vanýsek, P.; Buck, R. P. *J. Electroanal. Chem. Interfacial Electrochem.* **1984**, *163*, 1−9.
(20) Mareček, V.; Samec, Z.; Koryta, J. *Adv. Colloid Interface Sci.* **1988**, *29*, 1−78.
(21) Senda, M.; Kakiuchi, T.; Osaka, T. *Electrochim. Acta* **1991**, *36*, 253−262.
(22) Stephenson, M. J.; Holmes, S. M.; Dryfe, R. A. W. *Electrochem. Commun.* **2004**, *6*, 294−298.
(23) Jing, P.; Zhang, M.; Hu, H.; Xu, X.; Liang, Z.; Li, B.; Shen, L.; Xie, S.; Pereira, C. M.; Shao, Y. *Angew. Chem., Int. Ed.* **2006**, *45*, 6861−6864.
(24) Shao, Y.; Mirkin, M. V.; Rusling, J. F. *J. Phys. Chem. B* **1997**, *101*, 3202−3208.
(25) Rastgar, S.; Pilarski, M.; Wittstock, G. *Chem. Commun.* **2016**, *52*, 11382−11385.
(26) Gschwend, G. C.; Olaya, A.; Peljo, P.; Girault, H. H. *Curr. Opin. Electrochem.* **2020**, *19*, 137−143.
(27) Samec, Z. *Pure Appl. Chem.* **2004**, *76*, 2147−2180.
(28) Marcus, R. A. *J. Chem. Phys.* **2000**, *113*, 1618−1629.
(29) Chen, R.; Xu, K.; Shen, M. *Electrochim. Acta* **2020**, *357*, 136788.
(30) Wang, Y.; Kakiuchi, T.; Yasui, Y.; Mirkin, M. V. *J. Am. Chem. Soc.* **2010**, *132*, 16945−16952.
(31) Shen, M.; Qu, Z.; DesLaurier, J.; Welle, T. M.; Sweedler, J. V.; Chen, R. *J. Am. Chem. Soc.* **2018**, *140*, 7764−7768.
(32) Colombo, M. L.; Sweedler, J. V.; Shen, M. *Anal. Chem. (Washington, DC, U.S.)* **2015**, *87*, 5095−5100.
(33) Osakai, T.; Okamoto, M.; Sugihara, T.; Nakatani, K. *J. Electroanal. Chem.* **2009**, *628*, 27−34.
(34) Quinn, B.; Lahtinen, R.; Murtomäki, L.; Kontturi, K. *Electrochim. Acta* **1998**, *44*, 47−57.
(35) Ulmeanu, S. M.; Jensen, H.; Samec, Z.; Bouchard, G.; Carrupt, P.-A.; Girault, H. H. *J. Electroanal. Chem.* **2002**, *530*, 10−15.
(36) Samec, Z.; Langmaier, J.; Trojánek, A. *J. Electroanal. Chem.* **1997**, *426*, 37−45.
(37) Samec, Z.; Langmaier, J.; Trojánek, A. *J. Electroanal. Chem.* **1996**, *409*, 1−7.
(38) Langmaier, J.; Samec, Z. *J. Electroanal. Chem.* **2002**, *528*, 77−81.
(39) Samec, Z.; Trojánek, A.; Samcová, E. *J. Electroanal. Chem.* **1995**, *386*, 225−228.
(40) Zdrachek, E.; Bakker, E. *Anal. Chem.* **2020**, *92*, 2926−2930.
(41) Zou, X. U.; Chen, L. D.; Lai, C.-Z.; Bühlmann, P. *Electroanalysis* **2015**, *27*, 602−608.
(42) Deryabina, M. A.; Hansen, S. H.; Jensen, H. *Anal. Chem.* **2011**, *83*, 7388−7393.
(43) Zolotov, S. A.; Vladimirova, E. V.; Dunaeva, A. A.; Shipulo, E. V.; Petrukhin, O. M.; Vatsuro, I. M.; Kovalev, V. V. *Russ. J. Electrochem.* **2014**, *50*, 940−946.
(44) Nakatani, K.; Yamashita, J.; Negishi, T.; Osakai, T. *J. Electroanal. Chem.* **2005**, *575*, 27−32.
(45) Wilke, S.; Zerihun, T. *J. Electroanal. Chem.* **2001**, *515*, 52−60.
(46) Quinn, B.; Lahtinen, R.; Kontturi, K. *J. Electroanal. Chem.* **1997**, *436*, 285−290.
(47) Hossain, M. M.; Girault, H. H.; Lee, H.-J. *Bull. Korean Chem. Soc.* **2012**, *33*, 1734−1740.
(48) Laaksonen, T.; Ahonen, P.; Kontturi, K.; Murtomäki, L. *J. Electroanal. Chem.* **2005**, *575*, 75−80.
(49) Tavakolian-Ardakani, Z.; Hosu, O.; Cristea, C.; Mazloum-Ardakani, M.; Marrazza, G. *Sensors* **2019**, *19*, 2037.
(50) Taly, A.; Corringer, P.-J.; Guedin, D.; Lestage, P.; Changeux, J.-P. *Nat. Rev. Drug Discovery* **2009**, *8*, 733−750.
(51) Lozier, B. K.; Haven, T. R.; Astill, M. E.; Hill, H. R. *Am. J. Clin. Pathol.* **2015**, *143*, 186−192.
(52) Luchicchi, A.; Bloem, B.; Viaña, J. N. M.; Mansvelder, H. D.; Role, L. W. *Front. Synaptic Neurosci.* **2014**, *6*, 24.

(53) Jaramillo, A.; Lopez, S.; Justice, J. B.; Salamone, J. D.; Neil, D. B. *Anal. Chim. Acta* **1983**, *146*, 149−159.
(54) Mitchell, K. M. *Anal. Chem.* **2004**, *76*, 1098−1106.
(55) Marty, J.-L.; Sode, K.; Karube, I. *Anal. Chim. Acta* **1990**, *228*, 49−53.
(56) Doretti, L.; Ferrara, D.; Lora, S.; Schiavon, F.; Veronese, F. M. *Enzyme Microb. Technol.* **2000**, *27*, 279−285.
(57) Hou, S.; Ou, Z.; Chen, Q.; Wu, B. *Biosens. Bioelectron.* **2012**, *33*, 44−49.
(58) Wu, Y.; Wu, J.; Jiao, L.; Xu, W.; Wang, H.; Wei, X.; Gu, W.; Ren, G.; Zhang, N.; Zhang, Q.; Huang, L.; Gu, L.; Zhu, C. *Anal. Chem.* **2020**, *92*, 3373−3379.
(59) Liu, C.; Shen, Y.; Yin, P.; Li, L.; Liu, M.; Zhang, Y.; Li, H.; Yao, S. *Anal. Biochem.* **2014**, *465*, 172−178.
(60) Wang, C.-I.; Chen, W.-T.; Chang, H.-T. *Anal. Chem.* **2012**, *84*, 9706−9712.
(61) Shimomura, T.; Itoh, T.; Sumiya, T.; Mizukami, F.; Ono, M. *Enzyme Microb. Technol.* **2009**, *45*, 443−448.
(62) Wang, X.-F.; Zhou, Y.; Xu, J.-J.; Chen, H.-Y. *Adv. Funct. Mater.* **2009**, *19*, 1444−1450.
(63) Guerrieri, A.; Palmisano, F. *Anal. Chem.* **2001**, *73*, 2875−2882.
(64) Doretti, L.; Gattolin, P.; Burla, A.; Ferrara, D.; Lora, S.; Palma, G. *Appl. Biochem. Biotechnol.* **1998**, *74*, 1−12.
(65) Ying, T. S.; Bee, O. K. *J. Biosci.* **1997**, *8*, 64−70.
(66) Huang, T.; Yang, L.; Gitzen, J.; Kissinger, P. T.; Vreeke, M.; Heller, A. *J. Chromatogr. B: Biomed. Sci. Appl.* **1995**, *670*, 323−327.
(67) Navera, E. N.; Sode, K.; Tamiya, E.; Karube, I. *Biosens. Bioelectron.* **1991**, *6*, 675−680.
(68) Tamiya, E.; Sugiura, Y.; Nepomuceno Navera, E.; Mizoshita, S.; Nakajima, K.; Akiyama, A.; Karube, I. *Anal. Chim. Acta* **1991**, *251*, 129−134.
(69) Teelken, A. W.; Schuring, H. F.; Trieling, W. B.; Damsma, G. *J. Chromatogr. B: Biomed. Sci. Appl.* **1990**, *529*, 408−416.
(70) Niwa, O.; Horiuchi, T.; Kurita, R.; Torimitsu, K. *Anal. Chem.* **1998**, *70*, 1126−1132.
(71) Guerrieri, A.; Lattanzio, V.; Palmisano, F.; Zambonin, P. G. *Biosens. Bioelectron.* **2006**, *21*, 1710−1718.
(72) Karube, I.; Yokoyama, K.; Tamiya, E. *Biosens. Bioelectron.* **1993**, *8*, 219−228.
(73) Chen, Q.; Kobayashi, Y.; Takeshita, H.; Hoshi, T.; Anzai, J.-i. *Electroanalysis* **1998**, *10*, 94−97.
(74) Garguilo, M. G.; Huynh, N.; Proctor, A.; Michael, A. C. *Anal. Chem.* **1993**, *65*, 523−528.
(75) Morelis, R. M.; Coulet, P. R. *Anal. Chim. Acta* **1990**, *231*, 27−32.
(76) Tamiya, E.; Karube, I. Ultramicro-Biosensors For Monitoring Of Neurotransmitters. In *Neurobionics*; Bothe, H.-W., Samii, M., Eckmiller, R., Eds.; Elsevier: Amsterdam, 1993; pp 279−288.
(77) Zhang, Z.; Wang, J.; Wang, X.; Wang, Y.; Yang, X. *Talanta* **2010**, *82*, 483−487.
(78) Moscone, D.; D'Ottavi, D.; Compagnone, D.; Palleschi, G.; Amine, A. *Anal. Chem.* **2001**, *73*, 2529−2535.
(79) Blum, L. J.; Coulet, P. R. *Biosensor Principles and Applications*; Marcel Dekker Inc.: New York, 1991.
(80) Peteu, S. F.; Emerson, D.; Mark Worden, R. A. *Biosens. Bioelectron.* **1996**, *11*, 1059−1071.
(81) Martín-Barreiro, A.; de Marcos, S.; de la Fuente, J. M.; Grazú, V.; Galbán, J. *Sens. Actuators, B* **2018**, *277*, 261−270.
(82) Rahimi, P.; Joseph, Y. *TrAC, Trends Anal. Chem.* **2019**, *110*, 367−374.
(83) Lin, S.; Liu, C.-C.; Chou, T.-C. *Biosens. Bioelectron.* **2004**, *20*, 9−14.
(84) Murugan, C.; Murugan, N.; Sundramoorthy, A. K.; Sundaramurthy, A. *ACS Appl. Nano Mater.* **2020**, *3*, 8461−8471.
(85) Dutta, J. C.; Sharma, P. K. *IEEE Sens. J.* **2018**, *18*, 3090−3097.
(86) Sharma, P. K.; Thakur, H. R.; Dutta, J. C. *J. Comput. Electron.* **2017**, *16*, 584−592.
(87) Buiculescu, R.; Chaniotakis, N. A. Semiconductor Quantum Dots as Highly Effective Biosensing Tools. *CAS 2012 (International Semiconductor Conference)*, 2012; pp 87−90.
(88) Nyamsi Hendji, A. M.; Jaffrezic-Renault, N.; Martelet, C.; Shul'ga, A. A.; Dzydevich, S. V.; Soldatkin, A. P.; El'skaya, A. V. *Sens. Actuators, B* **1994**, *21*, 123−129.
(89) Tran-Minh, C.; Pandey, P. C.; Kumaran, S. *Biosens. Bioelectron.* **1990**, *5*, 461−471.
(90) Eppelsheim, C.; Hampp, N. *Analyst* **1994**, *119*, 2167−2171.
(91) Durand, P.; David, A.; Thomas, D. *Biochim. Biophys. Acta, Enzymol.* **1978**, *527*, 277−281.
(92) Bard, A. J.; Faulkner, L. R. *Electrochemical Methods Fundamental and Applications*, 2nd ed.; Wiley, 2001.
(93) Guo, J.; Amemiya, S. *Anal. Chem.* **2006**, *78*, 6893−6902.
(94) Welle, T. M.; Alanis, K.; Colombo, M. L.; Sweedler, J. V.; Shen, M. *Chem. Sci.* **2018**, *9*, 4937−4941.
(95) Wang, Y.; Velmurugan, J.; Mirkin, M. V.; Rodgers, P. J.; Kim, J.; Amemiya, S. *Anal. Chem.* **2010**, *82*, 77−83.
(96) Shen, M.; Ishimatsu, R.; Kim, J.; Amemiya, S. *J. Am. Chem. Soc.* **2012**, *134*, 9856−9859.
(97) Zoski, C. G.; Mirkin, M. V. *Anal. Chem.* **2002**, *74*, 1986−1992.
(98) Rodgers, P. J.; Amemiya, S. *Anal. Chem.* **2007**, *79*, 9276−9285.
(99) Harris, D. C. *Quantitative Chemical Analysis*, 9th ed.; W. H. Freeman and Company: New York, 2016.
(100) Langmaier, J.; Trojánek, A.; Samec, Z. *J. Electroanal. Chem.* **2008**, *616*, 57−63.
(101) Valent, O.; Koryta, J.; Panoch, M. *J. Electroanal. Chem. Interfacial Electrochem.* **1987**, *226*, 21−25.
(102) Rodgers, P. J.; Amemiya, S.; Wang, Y.; Mirkin, M. V. *Anal. Chem.* **2010**, *82*, 84−90.
(103) Kakiuchi, T. *J. Electroanal. Chem.* **1992**, *322*, 55−61.
(104) Kontturi, K.; Manzanares, J. A.; Murtomäki, L.; Schiffrin, D. J. *J. Phys. Chem. B* **1997**, *101*, 10801−10806.
(105) Li, Q.; Xie, S.; Liang, Z.; Meng, X.; Liu, S.; Girault, H. H.; Shao, Y. *Angew. Chem., Int. Ed.* **2009**, *48*, 8010−8013.
(106) Cai, C.; Tong, Y.; Mirkin, M. V. *J. Phys. Chem. B* **2004**, *108*, 17872−17878.
(107) Schmickler, W. *J. Electroanal. Chem.* **1997**, *426*, 5−9.
(108) Ammann, D. *Ion-Selective Microelectrodes*; Springer: Berlin, 1986; pp 55.
(109) Gulaboski, R.; Galland, A.; Bouchard, G.; Caban, K.; Kretschmer, A.; Carrupt, P.-A.; Stojek, Z.; Girault, H. H.; Scholz, F. *J. Phys. Chem. B* **2004**, *108*, 4565−4572.
(110) *CRC Handbook of Chemistry and Physics*, 87 ed.; Taylor & Francis, 2006.

https://doi.org/10.1021/acs.analchem.1c03711
Anal. Chem. XXXX, XXX, XXX−XXX